EUROPEAN COOPERATION
IN THE FIELD OF SCIENTIFIC
AND TECHNICAL RESEARCH

EURO-COST

COST 273 TD(03)200
Prague, Czech
September 24-26, 2003

SOURCE: Graduate School of Science and Engineering
Tokyo Institute of Technology-JAPAN

Estimation and Modeling of Non-specular Wave Scattering from Building Surface Using Superresolution Technique

Hary Budiarto, Kenshi Horihata,
Katsuyuki Haneda and Jun-ichi Takada
2-12-1 O-okayama
Meguro-ku Japan 152-8552
Phone: +81 3-5734-3288
Fax: +81 3-5734-3288
Email: hary@ap.ide.titech.ac.jp, knc@rose.zero.ad.jp,
haneda@ap.ide.titech.ac.jp, takada@ide.titech.ac.jp

Estimation and Modeling of Non-specular Wave Scattering from Building Surface Using Superresolution Technique

Hary Budiarto, Kenshi Horihata, Katsuyuki Haneda and Jun-ichi Takada
Graduate School of Science and Engineering, Tokyo Institute of Technology-JAPAN

September 15, 2003

Abstract

Multipath prediction with respect to a building surface has been conventionally based on an assumption that the scattering point from the surface has a substantial specular direction. However non-specular scattering from the building surface can affect the channel characteristics as well as specular scattering. This paper presents multipath characteristics of non-specular wave scattering from building surface roughness based on the experimental results. Superresolution method was applied as an approach to handle the signal parameters (DoA, ToA) of the individual incoming waves reflected from building surface roughness.

1 Introduction

In urban areas, buildings are the dominant scatterers determining propagation properties. The propagation prediction must reliably predict the influence of buildings and other obstructions. Microscopic scattering models are required to reflect the properties of the environmental objects [7][8]. If they are not adequately modeled, the propagation prediction can result in large errors. Reflection, diffraction, and scattering of the electromagnetic waves on the building surfaces in the radio environment induce undesirable multipath propagation. Consequently, the transmitted signal reaches the receiver through different propagation paths. Multipath prediction on a building surface was conventionally based on specular reflected wave. However, the multipaths are also generated by scattered waves propagating in non-specular directions. Therefore, non-specular scattering from the building surface can also affect the channel characteristics as well as specular scattering [1]. In order to predict the channel characteristic in more detail, multipath propagation of microscopic scattering is important [2]. This paper presents multipath characteristics of non-specular wave scattering from the building surface roughness based on experimental results. The antenna element was scanned spatially to detect the directions of arrival (DoA) and the carrier frequency was scanned to obtain the times of arrival (ToA). Superresolution method was applied as an approach to handle the signal parameters (DoA, ToA) of the individual incoming waves scattered from building surface roughness. The results show that the multiple paths can be detected at many scatterers, such as ground, window's glass, window's frames, bricks surface, as well as directly from the transmitter. The signal parameters of the arrival waves from the building scatterer are categorized as specular reflection, specular diffraction and diffusse scattering. The non-specular scattering from building surfaces is more dominated by windows scatterers than by brick scatterers.

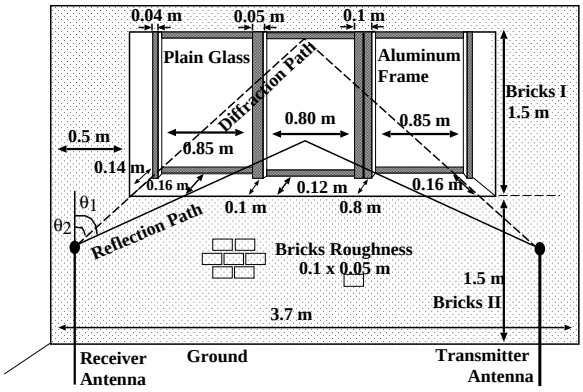

Figure 1: Building The Surface Profile

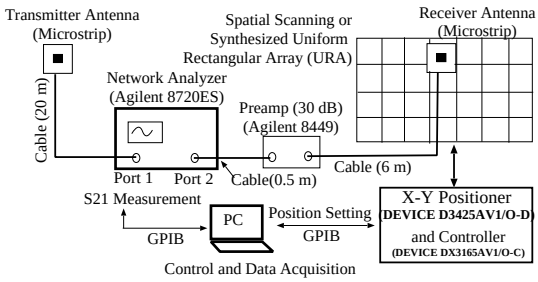

Figure 2: The Equipment Arrangement

2 Environment Consideration

2.1 Building Surface Profile

The profile of the building surface is shown in figure 1. The profile was taken from one of the buildings at Tokyo Institute of Technology. The surface of the building has non-uniformity due to the windows (glass), frames (aluminum), and walls (bricks). The surface has periodical irregularity of five periods. One period of the surface equals 3.7 m. The windows are made up of the sidewall, aluminum frames and plain glasses, which in principle are the building roughness, as well as the wall surface. The dimensions of the window's glasses of the building are 0.85×1.5 m^2, 0.8×1.5 m^2, and 0.85×1.5 m^2. The three different window frames have outer dimensions of 0.04×1.5 m^2, 0.05×1.5 m^2 and 0.10×1.5 m^2. The first and the third window frames have the same offset depth of 0.16 m different from the second window frame that has 0.12 m offset depth. The windows are elevated 1.5 m from the ground. The wall surface, that has periodical roughness in both horizontal and vertical directions, is made of 0.1×0.05 m^2 bricks with 0.01 m gap among each other.

2.2 Transmitter and Receiver Models

The transmitter and receiver antennas were linearly polarized rectangular microstrip antennas with ground plane size of 0.08×0.08 m^2. The patch size was 0.0179×0.0179 m^2 on a dielectric substrate with $\epsilon_r = 2.55$. The center frequency of the antennas was 4.95 GHz with bandwidth of 180 MHz. The wavelength was comparable with or smaller than depth of building surface roughness. The receiver antenna was shifted spatially by a X-Y positioner to obtain field strength at each point in the scanning region. Both antennas were aligned to transmit and receive vertical polarization. The height of the transmitter antenna was 1.9 m from ground. The transmitter antenna was fixed at 2.7 m away in front of the building surface. Figure 2 shows the arrangement of the experiment [6]. The transfer function between transmitter and receiver antennas was measured using a Vector Network Analyzer (VNA).

The X-Y positioner was used for automatic scanning of the receiver antenna. The measurement of the frequency characteristics of the transfer function and the shifting of receiver antenna were operated automatically using a personal computer through the positioner controller and General Purpose Interface Bus (GPIB) to achieve high accuracy and easy measurement. The X-Y positioner has an accuracy of 1 mm. Table 1 shows the detailed parameters of the experiments.

Table 1: Experimental Parameter

Antennas	Tx & Rx Microstrip Reflection coefficient is bellow -10 dB in $4.85 - 5.05$ GHz. Beam width in E and H planes are 45°
Measurement Points	Spatially 10 $\times$10 points (25 mm interval), 21 points over frequency $(4.85 - 5.05$ GHz).
Snapshot	20 times
Estimations Parameters	The number of waves and each wave's azimuth, elevation, delay and path gain
Signal processing	LS 3-D Unitary ESPRIT
Smoothing in ESPRIT	Spatially 4 times and 7 times over frequency
Wave Polarization	Vertical-Vertical
Normalization	Face-to-face, the distance between Tx and Rx is 1 m at experiment location

2.3 The Spatial Scanning Model

The spatial scanning was configured to resemble an array antenna, also called synthesized uniform rectangular array (URA). The measurement points during the spatial scanning were discretized for every 0.025 m toward the horizontal and vertical directions. The measurement was performed along 0.5 m in the vertical direction. The middle of the vertical direction scanning region was at the same height as the transmitter antenna. Figure 3 illustrates top view of the spatial scanning model. The spatial scanning performs the measurement 8.125 m along the horizontal direction. The transmitter antenna is positioned facing towards the bricks' surface of the building. The first vertical direction of measurement is 0.7 m away from the transmitter antenna, which corresponds to 10° incident angle in the specular direction.

3 Data Processing

3.1 Data Measurements

Since the VNA also measures the transfer functions of the cable and amplifier, calibration of the data measurement system is required to eliminate the effect of the equipment. The transfer function of the signal was measured using a network analyzer with the frequency range from 4.85 to 5.05 GHz. The transfer function measured by the VNA can be expressed as follows.

$$X(f) = H(f) \times G(f) \tag{1}$$

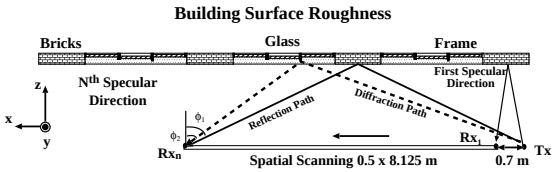

Figure 3: Top View of the Spatial Scanning Model

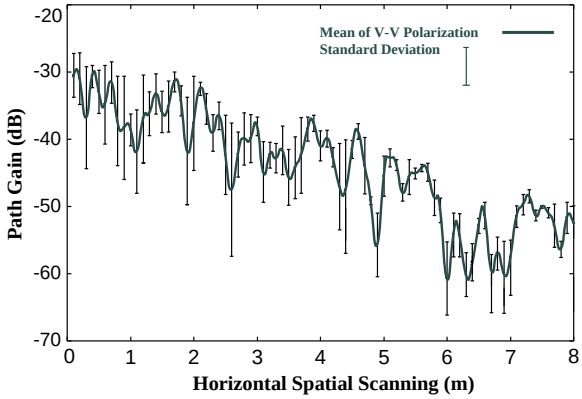

Figure 4: Mean Value and Standard Deviations of Data Measurement

where $G(f)$ is the transfer function of the cable, amplifier and antenna complex directivity at broadside, and $H(f)$ is the Friis free space transfer function, which is given as,

$$H(f) = \frac{\lambda}{4\pi d} \exp(-j\frac{2\pi}{\lambda}d) \tag{2}$$

where d is the propagation path, and λ is the wavelength. All measurement data resulted from this experiment was already calibrated by applying function $G(f)$, which was obtained from the measurement using the transmitter and receiver antennas positioned face-to-face with 1 m distance from each other, in an open space. Figure 4 shows mean values and standard deviations of data measurement for V-V polarizations. Mean values and standard deviations were calculated from the vertical spatial scanning. The figure shows them in the errorbar graph with 0.1 m discretized at the horizontal spatial scanning.

3.2 Signal Processing

In order to obtain signal parameters of the arrival wave, measurement data are formulated. Suppose that L waves are impinging at the receiver have three parameters of azimuth angle $(\phi_l - \frac{\pi}{2})$, elevation angle $(\frac{\pi}{2} - \theta_l)$ and delay time τ_l, where $1 \leq l \leq L$. With the X-Y positioner, the receiver antenna performs spatial scanning both in the horizontal and vertical directions where the intervals of the sampling points are Δ_x and Δ_y. The numbers of sampling points are M_1 and M_2, respectively. At each sampling point, it carries out M_3 points of sampling over the frequency where the interval of sampling is Δ_f and the center frequency is f_c. If the electrical lengths of the aperture of the array, $\frac{2\pi}{\lambda_c}M_1\Delta_x$ and $\frac{2\pi}{\lambda_c}M_2\Delta_y$, are both sufficient to be assumed as constant within the bandwidth $M_3\Delta_f$, i.e, $M_1\Delta_x \cdot M_3\Delta_f \ll c$, and $M_2\Delta_y \cdot M_3\Delta_f \ll c$, where c is a light velocity, then the measured data y_{k_1,k_2,k_3} can be expressed as,

$$z_{k_1,k_2,k_3} = \sum_{l=1}^{L} \left[s_l \prod_{r=1}^{3} e^{j\mu_l^{(k_r)}} \right] + n_{k_1,k_2,k_3} \tag{3}$$

where $0 \leq k_r \leq (M_r - 1)$ $1 \leq r \leq 3$ indicates a location of each sampling point, n_{k_1,k_2,k_3} is a white Gaussian noise of zero mean, s_l is a complex amplitude of the l^{th} wave at a reference point and $\mu_l^{(r)}$ is denoted by

$$\mu_l^{(1)} = \frac{2\pi}{\lambda_c}\Delta_x \sin(\phi_l - \frac{\pi}{2}) \cos(\frac{\pi}{2} - \theta_l), \tag{4}$$

$$\mu_l^{(2)} = \frac{2\pi}{\lambda_c}\Delta_y \sin(\frac{\pi}{2} - \theta_l), \quad (5)$$

$$\mu_l^{(3)} = 2\pi\Delta_f \tau_l. \quad (6)$$

These values include parameters of the incident waves so that the objective is to obtain these L sets of 3-D mode parameters. Then, vectorization of data measurement can be defined as

$$\begin{aligned} \boldsymbol{z} = [&z_{1,1,1}\ z_{2,1,1} \dots z_{M_1,1,1}\ z_{1,2,1} \dots \\ &z_{M_1,M_2,1}\ z_{1,1,2} \dots z_{M_1,M_2,M_3}]^T \in C, \\ &= \boldsymbol{A}\boldsymbol{s} + \boldsymbol{n}, \end{aligned} \quad (7)$$

where $s \in C^L$ and $n \in C^M$ ($M = M_1M_2M_3$) are the complex amplitude vector and noise vector respectively. The multi-dimensional mode matrix $\boldsymbol{A} \in C^{M\times L}$ is generated by mode matrices each of which corresponds to a parameter as

$$\boldsymbol{A} = \boldsymbol{A}(\mu^{(3)}) \diamond \boldsymbol{A}(\mu^{(2)}) \diamond \boldsymbol{A}(\mu^{(1)}) \in C^{M\times L}, \quad (8)$$

where $\diamond$ denotes the kronecker product of each row of the matrices and

$$\boldsymbol{A}(\mu^{(r)}) = [\boldsymbol{a}(\mu_1^{(r)}) \dots \boldsymbol{a}(\mu_L^{(r)})] \in C^{M_r\times L}, \quad (9)$$

$$a(\mu_1^{(r)}) = [1\ e^{-j\mu_r^{(r)}} \dots e^{-j(M_r-1)\mu^{(r)}}]^T \in C^{M_r}. \quad (10)$$

The 3D unitary ESPRIT algorithm [5][6] was used to obtain the signal parameters. It is a superresolution direction finding method of the arrival wave. In physical terms, the ESPRIT is equivalent to finding out the parameters of the arrival wave using the phase difference between groups of uniformly positioned elements of sensor array. The ESPRIT array data had a size of (10×10) or (25×25) cm^2 for each observation point. The arrival wave analyses were performed at 60 observation points with an interval of 12.5 cm.

4 Signal Parameter Arrival Wave

The signal parameters of the arrival waves that can be obtained using ESPRIT are azimuth angle, elevation angle, delay time and path gain. If the azimuth and elevation angles of the arrival wave are known, then the propagation path from the transmitter to the receiver antenna can be determined. Therefore, the delay time based on free space velocity (3×10^8 m/s) of each path can be easily obtained. Additionally, by knowing the propagation path and difference between the delay time estimated by using ESPRIT result and the delay time estimated by using free space velocity result for each of arrival waves, double scattering can be distinguished. Azimuthal and elevation angles of specular reflection point, specular diffraction point and diffuse scattering point are required for detailed classification of typical paths. The specular diffraction satisfies the Keller's law of diffraction. The elevation and azimuthal for the typical path of reflection and diffraction angle are shown in figure 1 and figure 3, respectively.

Figure 5 and 6 show the ESPRIT result for an azimuthal and an elevation angle of the arrival wave, respectively . The line perpendicular to the x-axis depicts the range value of the azimuthal angle. The negative azimuthal angle, representing the wave, comes from the right-hand side of the receiver or source side (see figure 3). The legends in the figures show the type of scatterers. The number of icons on the vertical line corresponds to the number of multipath signals. Multiple paths can be detected from many scatterers, such as ground, bricks I, bricks II, windows glass or windows frames, and directly from the transmitter.

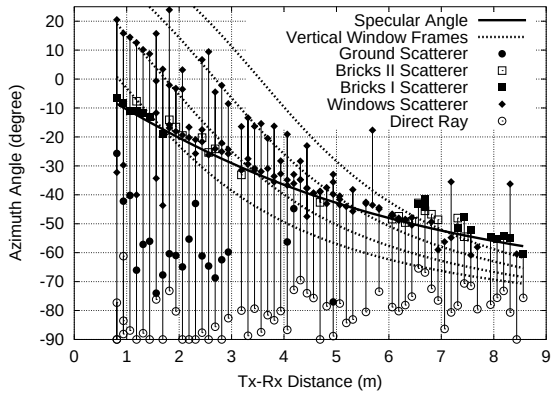

Figure 5: Azimuth Angle of Arrival Wave

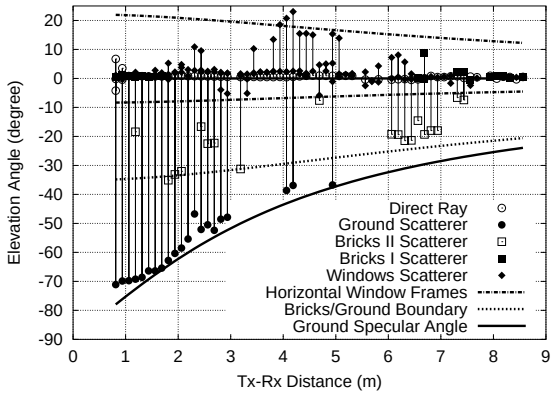

Figure 6: Elevation Angle of Arrival Wave

The types of brick scatterer are distinguished as the brick scatterer with height between the lower and upper part of the windows, classified as bricks-I, and the brick scatterer with height below the windows, classified as bricks-II. However, the ESPRIT result is not accurate enough to distinguish the arrival waves coming from window's glass, window's frame and boundary of windows's glass and frame. Therefore, they are called altogether as windows scatterer. Three categories of arrival wave namely reflected wave, diffracted wave and diffuse scattering can be observed from windows scatterer.

4.1 Specular Reflected Waves

Figure 5 and 6 show that most of the arrival waves from windows scatterer (window's glass) and bricks I are specular reflected waves. This is because the azimuthal angles have a tendency to be distributed arround the angle of specular direction and the elevation angle are around 0°. The figures also show that more than one scattered wave from windows scatterer was found from every observation point. Compare with arrival wave from bricks I, it was only one scattered for each observation point. This is due to the arrival waves from windows scatterer have two typical path as reflected path and diffracted path (see figure 1). Figure 7 shows path gain and delay time of the specular reflected waves from windows glass and bricks I. The delay time directly estimated by using ESPRIT yields close agreement with the delay time of the propagation path determined by using DoA estimated by ESPRIT and free space velocity. Average difference of delay time for glass scatterer and bricks I scatterer are 0.38 ns and 0.35 ns, respectively. It is noted that typical of propagation path is valid as reflected path. So that, the reflection coefficient of the glass surface and bricks surface can be estimated by specular reflected wave [3][4]. It will described more detail in the next section.

4.2 Diffraction Effect

Figure 5 shows the diffraction path from second vertical frame of windows at 1-2.5 m distance and third vertical frame of windows at 2.5-4.5 m distance. The elevation angle of the arrival waves are around 0°. This means that arrival waves are specular diffraction. Figure 6 also shows the diffraction effects are observed when the distance between transmitter and receiver antenna is 3.5-5 m with large elevation angle. It corresponds to the scattering point of specular diffraction from horizontal frame of windows. The angle of diffracted wave from vertical frame of windows and horizontal frame of windows that correspond by Keller's law of the diffraction. It is noted that the non-specular scattering from building surfaces is more dominated by frame of window scatterers than by brick

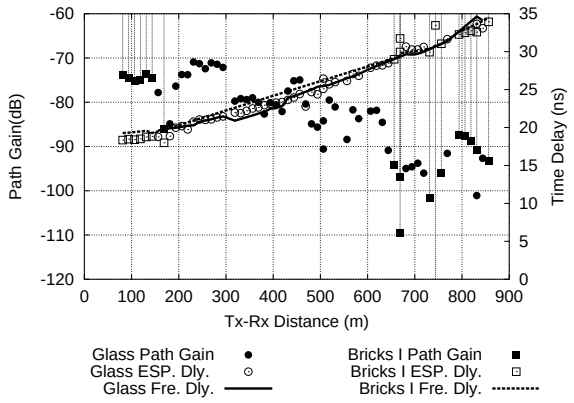

Figure 7: Path Gain and Delay Time Specular of the Reflected Waves

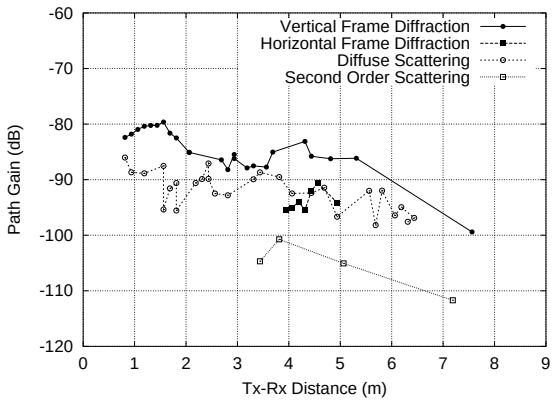

Figure 8: Path Gain of the Diffracted Wave, Diffuse Scattering and Second order Scattering

scatterers. However, the arrival wave of the window scatterers have a particular characteristic, i.e., when the observation point was close to the transmitter, the azimuth angles of the two arrival waves were varied at similar elevation angle for one observation point, in contrast to similar azimuth angle but different elevation angle when the observation point was at a distant point from the transmitter. Average deviation of the angle is 12° for both cases. This means, that when the observation is near the transmitter, the diffracted waves from vertical frame of windows are more dominant. and when the observation is at a distant point, the diffracted waves from horizontal frame of windows are more dominant. Figure 8 shows that the path gain of the specular reflected, specular diffracted, diffuse scattering and second order scattering are significant different. The path gain of horizontal window frames diffraction is lower than vertical window frame diffraction. The arrival waves are called as diffuse scattering, if it can not be included in the reflected wave or the diffracted wave. Second order scattering is observed when low path gain and large delay time. Figure 9 shows delay time and difference of path gain specular reflected wave and non-specular reflected wave such as diffracted, diffuse scattering and second order scattering. The average difference of delay time directly estimated by using ESPRIT and delay time of propagation path determined by using DoA estimated by ESPRIT and space velocity for windows scatterer are 0.83 ns. The value is larger in comparison to others scatterer due to the occurrence of second order scattering.

4.3 Ground Scattered

The arrival wave is specular ground-reflected wave when the angle of azimuth is $-90°$. Figure 6 shows that specular ground-reflected wave can not always be observed. This is possibly because the directivity of antenna toward the ground is rather small. Due to the antenna directivity the direct wave is more dominant. Therefore, the direct wave is observed in all measuring ranges. It is also possible that in Fig. 6, the elevation angle of specular ground-reflected wave approaches the elevation angle of the boundary between building and ground at distant points. Therefore, the specular ground-reflected might be classified as bricks II scattered waves. Figure 10 shows path gain and delay time of the ground scatterers and bricks II. The average difference of delay time estimated using ESPRIT and delay time of propagation path determined by DoA of ESPRIT and free space velocity are 0.38 ns and 0.51 ns for ground scatterer and bricks II, respectively.

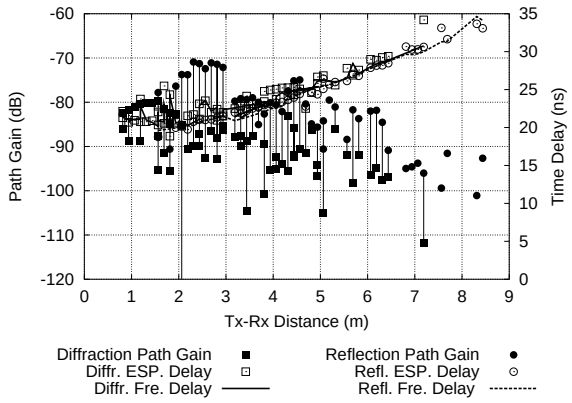

Figure 9: Path Gain and Delay Time of the Non-specular Windows Scatterer and Specular Windows Scatterer

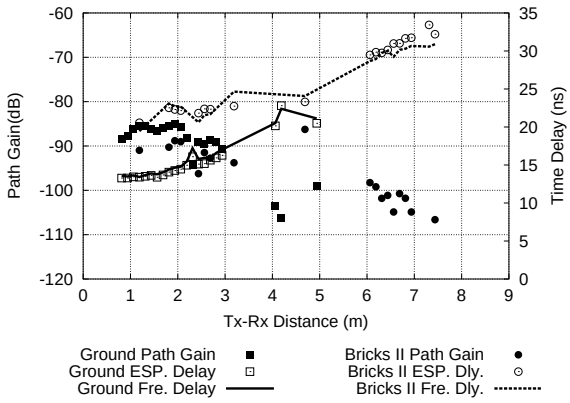

Figure 10: Path Gain and Delay Time of the Ground Scattered Waves and Bricks II

4.4 Direct Ray

Figure 5 shows that the arrival waves coming directly from the transmitter can be observed at all observation point. The first observation point located at 81.25 cm from the transmitter, six arrival waves were obtained, which consisted of two waves that arrive directly, one ground reflection and three waves from the building's surface. The reason why the two waves were directly obtained is because the distance between the transmitter and receiver is relatively close. Therefore, the receiver gets the reflection from the support of the antenna. This kind of result was only obtained at the first and second observation points. Figure 11 show path gain and delay time for direct waves. The deviation of path gain between direct waves and the others scatterer is less than 20 dB. It means that the signal from the others scatterer are not noise signal. The average difference of delay time estimated using ESPRIT and delay time of propagation path determined by DoA of ESPRIT and free space velocity are 0.25 ns.

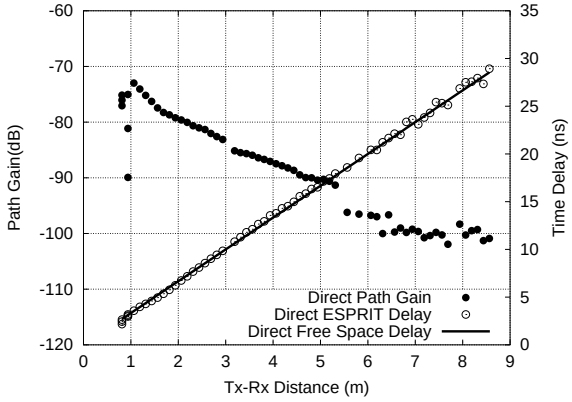

Figure 11: Path Gain and Delay Time of the Direct Waves

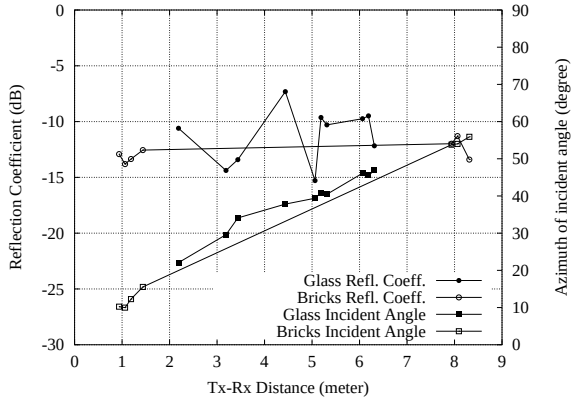

Figure 12: Reflection Coefficient for Glass and Bricks Building Surface

5 Reflection Coefficient Estimated

The reflection coefficient of the building surface can be estimated by using signal parameters of the arrival wave from the specular direction. According measurement loss, the

reflection coefficient can be estimated as follows:

$$TL = RC + G_t + G_r + 20\log_{10}\frac{\lambda}{4\pi d}, \tag{11}$$

where TL[dB] is total loss of the measurement, RC [dB] is reflection coefficient, G_t [dB] and G_r [dB], are directivities of the transmitter and the receiver antennas, respectively. The previous section is mentioned that the reflected wave arrive from glass surface and bricks surface. Therefore, reflection coefficient of glass surface and bricks surface can be estimated. Figure 12 shows reflection coefficient for glass surface and bricks surface. The incident angle of the reflection coefficients are shown y-right axis.

6 Conclusion

This paper presented the multipath characteristics of non-specular wave scattering from 3-D building surface roughness. The result shows that the multiple paths can be detected at many scatterers, such as ground, window's glass, window's frame, bricks surface, as well as directly from the transmitter. Three categories of arrival wave namely reflected wave, diffracted wave and diffuse scattering can be observed from windows scatterer. The signal parameters of the arriving waves from the building scatterer have a tendency to be distributed around the angle of specular direction. Therefore reflection coefficient of the building surface can be estimated. The delay time directly estimated by using ESPRIT yields close agreement with the delay time of the propagation path determined by using DoA estimated by ESPRIT and free space velocity. The non-specular scattering from building surfaces is more dominated by window frame scatterers than by brick scatterers.

References

[1] J. Takada, J. Fu, H. Zhu, and T. Kobayashi, "Spatio-Temporal Channel Characterization in a Sub-Urban Non-Line-of-Sight Microcellular Environment", IEEE J. Select. Areas in Comm., vol. 20, no. 3, pp.532-538, Apr. 2002.

[2] H. Budiarto, K. Horihata, K. Haneda and J. Takada, "Experimental study of Non-specular Wave Scattering from Building Surface Roughness for the mobile Propagation Modeling", IEICE Transactions on Communications (to be accepted).

[3] L. Orlando, J.F. Martin and T.S. Rappaport, " A Comparison of Theoretical and Empirical Reflection Coefficients for typical Exterior Wall Surafces in a Mobile Radio Environment", IEEE Trans. on Antenna and Propagation Vol. 44 No. 3 pp. 341-351, March 1996.

[4] A. Satoh and E. Ogawa, "An Evaluation Method for the Reflection Coeficient of Buildings Wall", Electronics and Communications in Japan, Part 1, vol. 73, no. 3, pp. 92-103, 1990.

[5] M. Haardt and J.A. Nossek, "Simultaneous Schur Decomposition of Several Nonsymmetric Matrices to achieve Automatic pairing in Multidimensional harmonic Retrieval problems", IEEE Trans. on Signal Processing, vol. 46 no. 1 pp. 161-169, Jan. 1998.

[6] K. Sakaguchi, J. Takada and K. Araki, "A Novel Architecture for MIMO Spatio-Temporal Channel Sounder," IEICE Transactions on Electronics, vol. E-86C, no. 3, pp. 436-441, Mar. 2002.

[7] M.O. Al-Nuami and M.S. Ding, "Prediction Models and Measurements of Microwave Signals Scattered from Buildings", IEEE Trans. on Antenna and Propagation, vol.42, No.8 pp. 1126-1137, August 1994.

[8] H.H. Xia, H.L. Bertoni, L.R. Maciel, A.L. Stewart an R. Rowe, "Radio propagation Characteristic for Line-Of-Sight Microcellular and Personal Communication", IEEE Trans. on Antenna and Propagation, vol. 41, no.10, pp. 1439-1447, Oct. 1993.